ARCTIC
VOL. 47, NO. 3 (SEPTEMBER 1994) P. 288–297

Comparison of *in situ* and AVHRR-Derived Broadband Albedo over Arctic Sea Ice

R.A. De ABREU,[1] J. KEY,[2] J.A. MASLANIK,[2] M.C. SERREZE[2] and E.F. LeDREW[1]

(Received 5 May 1993; accepted in revised form 4 November 1993)

ABSTRACT. Advanced Very High Resolution Radiometer (AVHRR) data are used to extract broadband sea ice surface albedos from narrowband channel 1 and 2 top of the atmosphere (TOA) radiances. Corrections for the intervening atmosphere, viewing geometry and sensor spectral response are applied to the satellite data. Atmospheric correction increases TOA albedos by 27 to 32%. After removing the effects of viewing geometry, surface albedo variability between orbits decreases. The satellite-derived surface albedo over snow-covered sea ice corrected for viewing geometry ranged from 0.68 to 0.82. The residual diurnal variability is attributed to uncertainties in the atmospheric and anisotropic corrections of the satellite data. After comparison with coincidental *in situ* measurements, AVHRR albedos corrected for the intervening atmosphere and viewing geometry agreed favorably with surface measurements. The high variability in surface measurements reflects the difficulty in measuring surface albedos over areas consistent with those of a typical AVHRR pixel. In order to develop a reliable methodology for using these satellite data to derive sea ice albedo, an improved understanding of both the atmosphere's behavior over the long path lengths common to the Arctic and the anisotropic nature of snow-covered sea ice reflectance is required. Furthermore, any seasonal characteristics of these factors must be addressed.

Key words: sea ice, albedo, remote sensing, AVHRR, anisotropy

RÉSUMÉ. On utilise des données obtenues par radiomètre perfectionné à très haute résolution pour extraire des albédos à large bande de la surface de la glace à partir de luminances du sommet de l'atmosphère du canal 1 et 2 à bande étroite. On applique aux données par satellite des corrections pour l'atmosphère intermédiaire, l'angle de prise de vue et la réponse spectrale des capteurs. La correction atmosphérique augmente les albédos du sommet de l'atmosphère de 27 à 32 p. cent. Après avoir éliminé l'influence de l'angle de prise de vue, la variabilité de l'albédo de la surface entre les orbites diminue. L'albédo de la surface obtenu par satellite sur la glace de mer couverte de neige après correction pour l'angle de prise de vue allait de 0,68 à 0,82. On attribue la variabilité résiduelle diurne à des incertitudes dans les corrections atmosphérique et anisotrope des données obtenues par satellite. Après comparaison avec des mesures correspondantes effectuées *in situ*, les albédos obtenus à l'aide du radiomètre perfectionné à très haute résolution et corrigés pour l'atmosphère intermédiaire et l'angle de prise de vue concordaient d'assez près avec les mesures effectuées à la surface même. La grande variabilité dans les mesures de surface reflète la difficulté qu'il y a à mesurer les albédos de surface dans des régions correspondant à celles d'un pixel typique obtenu à l'aide d'un radiomètre perfectionné à très haute résolution. De façon à développer une méthodologie fiable permettant d'utiliser ces données par satellite pour obtenir l'albédo de la glace de mer, on a besoin de mieux comprendre à la fois le comportement de l'atmosphère sur les grandes longueurs de couloir communes à l'Arctique et la nature anisotrope de la réflectance de la glace de mer couverte de neige. Il faut en outre tenir compte de toute caractéristique saisonnière pertinente à ces facteurs.

Mots clés: glace de mer, albédo, télédétection, radiomètre perfectionné à très haute résolution, anisotropie

Traduit pour la revue *Arctic* par Nésida Loyer.

INTRODUCTION

Sea ice albedo controls the amount of incident solar energy absorbed into the snow–ice–ocean medium. Over polar surfaces, variations in surface albedo have significance for both climatological and biological processes. Surface albedo is a complicated function of surface and sub-surface optical properties, solar zenith angle, incident solar flux, and cloud cover (Warren, 1982). While remaining high for much of the polar year, the arctic albedo decreases dramatically during summer and becomes highly variable both spatially and temporally. The well-known *sea ice–albedo feedback* exemplifies the intimacy between sea ice cover and climate. Introduced formally by Budyko (1969) and Sellers (1969), the possibility of a positive feedback mechanism between sea ice and surface albedo has been identified as a major contributor to the sensitivity of the Arctic in various climate change scenarios (e.g., $2 \times CO_2$) simulated in general circulation models (Cubasch and Cess, 1990). Overly simplistic representations of sea ice albedo in climate models can lead to inconsistent and/or unrealistic simulations in the arctic regions. These crude parameterizations often reflect an incomplete understanding of surface and atmospheric contributions to sea ice albedo, a dearth of surface observational data, and an absence of a reliable procedure to map and monitor sea ice albedo at the temporal and spatial resolutions capable of representing the quantity's critical seasonal and spatial variance. Remote sensing

[1] Department of Geography and the Earth Observations Laboratory, Institute for Space and Terrestrial Science, University of Waterloo, Waterloo, Ontario N2L 3G1, Canada
[2] Cooperative Institute for Research in Environmental Sciences, University of Colorado, Campus Box 449, Boulder, Colorado 80309, U.S.A.

provides a way of improving our understanding and representation of albedo variations. The relative inaccessibility and harsh environmental conditions of the arctic make it an ideal candidate for remote observation.

Regular satellite coverage of the polar regions is currently provided by the National Oceanographic and Atmospheric Administration (NOAA) 11 and 12 satellites equipped with the Advanced Very High Resolution Radiometer (AVHRR). The TIROS NOAA family of sun-synchronous satellites has operated in near-polar orbits since 1978. The orbit allows all locations to be sampled at least twice a day at a nominal resolution of approximately 1.1 km at nadir (Kidwell, 1991). The AVHRR sensor consists of two visible channels and three thermal infrared channels (1: 0.58–0.68 μm; 2: 0.73–1.1μm; 3: 3.55–3.93 μm; 4: 10.3–11.3 μm; 5: 11.5–12.5 μm). The use of orbital data collected in the solar spectrum (0.29–4.0 μm) for determining surface radiation fluxes such as albedo has received much attention (Stephens *et al.,* 1981; Carleton, 1991). AVHRR's moderate spatial resolution and timely coverage have attracted a considerable share of this study. AVHRR-measured narrow band, visible radiances (chs. 1 and 2) at the top of the atmosphere (TOA) have been used to determine surface albedo (Gutman, 1988; Saunders, 1990). Much of this work, however, has focused on terrestrial surfaces at lower latitudes and relatively little effort has been given to extracting similar information for the polar regions. The uses of optical sensors in the Arctic are somewhat limited due to the frequent springtime cloud cover. Clear sky events, however, offer the opportunity to measure surface albedo at solar wavelengths. This paper represents a preliminary step towards developing a reliable methodology to extract broadband surface albedos over snow-covered sea ice surfaces using AVHRR-measured TOA radiances. Satellite-derived broadband albedos are compared to *in situ* surface broadband albedo measurements collected coincident to the acquisition of satellite data, and issues requiring further study are identified.

SITE DESCRIPTION

The study site was restricted to the First-year Ice Site (FYI) of the Sea Ice Monitoring and Modeling Site (SIMMS) experiment in the spring of 1992. The site was located at 74˚41.1′N and 95˚35.22′W in Resolute Passage in the Canadian Archipelago. For a full description of the site and experiment see LeDrew and Barber (1994) in this issue and Reddan *et al.* (1992). The site consisted of fast first-year sea ice that was covered by snow throughout this investigation. Over the period of study, this snowpack ranged in depth from 11–51 cm (T. Papakyriakou, pers. comm. 1993). Measurements of the surface's energy balance and geophysical properties were made throughout the experiment. Atmospheric conditions were monitored through surface observations at the site and at the nearby Atmospheric Environment Service (AES) Resolute Bay weather station. At the FYI site, a 1 km × 1 km grid was defined to allow surface albedo measurements to be made over an area approximately the size of an AVHRR pixel at nadir. Surface albedo observations were also made over a 500 m × 500 m Synthetic Aperture Radar (SAR) grid located approximately adjacent to the AVHRR grid.

METHODS

Surface Measurement of Sea Ice Albedo

Surface albedo was measured hourly from a tower at the FYI site and coincidentally with daily AVHRR passes within the 1 km × 1 km grid. At the site tower, a downward and upward-looking Epply Precision Spectral Pyranometer (PSP) measured the downward and upward flux over the spectral range 0.285–2.8 μm with an error of ±2.3% (Latimer, 1972). The pyranometer measuring incident flux was mounted 1.5 m above the ground, while the reflected short-wave flux was measured by an identical instrument suspended 8.9 m above the surface. All pyranometers were calibrated by AES before and after field use. No correction for tower shading has been applied to the data, but comparisons to ground-based measurements have revealed differences well within the instrument error.

Over the course of the experiment, spatial albedo measurements were made coincident with AVHRR overpasses within the sample grid using two different tripod-mounted instruments: a Middleton CN-9 Pyrano-albedometer (0.3–2.6 μm) and a customized albedometer consisting of upward- and downward-pointing LI-COR Terrestrial Pyranometers (0.4–1.2 μm). Given the prevalent illumination conditions, the CN-9 and LI-COR instruments are accurate to ±4% and ±7% respectively. Comparisons with albedos derived from the pyrano-albedometer showed the LI-COR sensor to be within ±2% of the glass-domed instrument. The grid was sampled on both clear and cloudy days, often coincidentally with NOAA overpasses. In order to determine the spatial variability of surface albedo over the grid, sampling transects were made in orthogonal directions. Each sample site was 200 m apart with 5–10 albedo measurements collected at each site.

Satellite-Derived Broadband Albedo

NOAA 11 and 12 AVHRR Local Area Coverage (LAC) data were provided by the Atmospheric Environment Service. With the two satellites, the SIMMS experiment area was covered with 10-12 orbits every 24 hours. Image sectors of 512 × 512 pixels centered over Resolute Bay were extracted. The spatial resolution of LAC data is dependent upon the location of the pixel in the swath. Data collected at nadir have a nominal spatial resolution of 1.1 km and become more coarse with distance from nadir. A full description of the NOAA platform and AVHRR sensor can be found in Kidwell (1991). Four clear-sky NOAA 12 orbits were chosen on Julian Day 134 (May 13) for detailed analysis (see Table 1).

The processing methodology for the selected orbits is shown schematically in Figure 1. Clear sky conditions were determined from both a visual analysis of all five channels and surface observations coincidental with the overpass. Ground observations indicate that high cirrus and diamond dust events may have slightly obscured the solar disk during orbits 5186 and 5187. Six

TABLE 1. Day 134 AVHRR data summary.

Orbit	Solar Time	Satellite Zenith	Satellite Azimuth	Solar Zenith	Solar Azimuth
5186	8.89	-23.34	112.86	60.93	130.77
5187	10.74	20.9	317.04	57.12	158.19
5188	12.20	42.58	341.53	56.23	186.53
5191	17.23	0.16	55.18	69.62	265.87

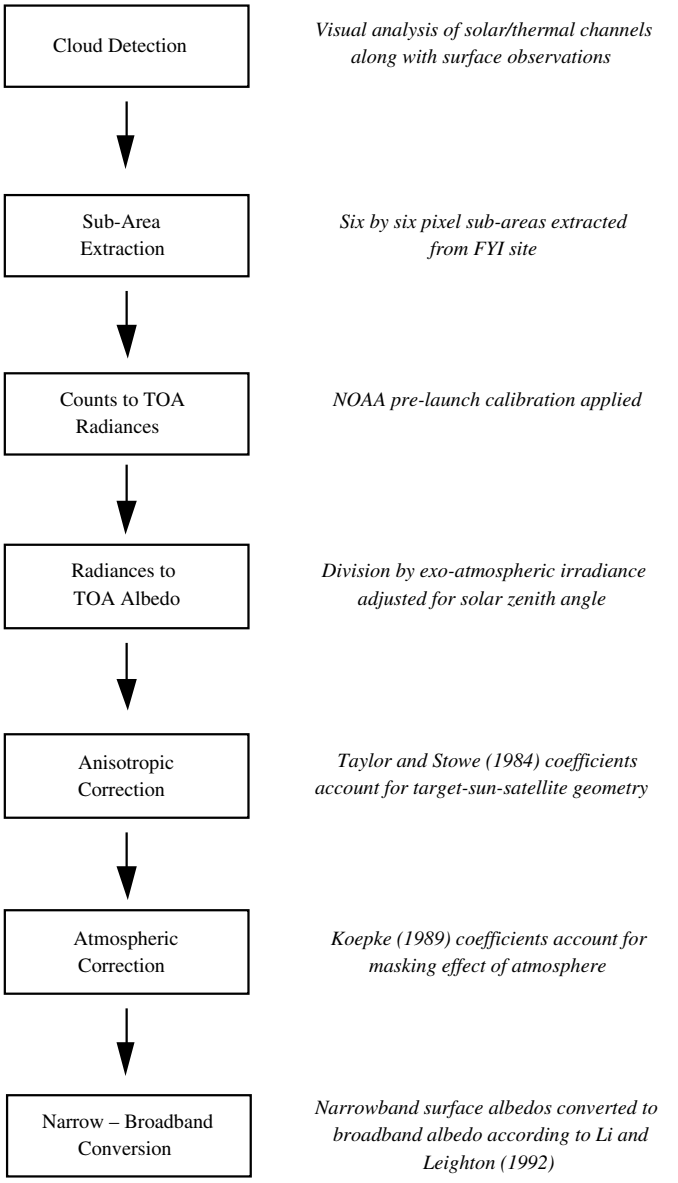

FIG. 1. AVHRR processing methodology.

by six pixel sub-areas that encompass the FYI site were extracted from the visible (ch. 1) and near-infrared (ch. 2) channels of each pass. These data were not geometrically rectified and registered to a common projection; thus, the size and geographic location of the subareas are considered similar but not identical between orbits. However, allowing for the relative homogeneity of the snow surface at that time of year and given the objective of this analysis, errors arising from the difference in subarea sizes and locations are considered small. Orbital (satellite zenith and azimuth angles) and celestial (solar zenith and azimuth angles) parameters for the nearby scene center were used for the study areas located approximately 15 km away. The effect on the satellite-derived results is thus considered minimal.

Calibration of Raw Digital Numbers: The raw counts or digital numbers (DNs) of each pixel were converted to TOA radiances (L_i) ($Wm^{-2}\,sr^{-1}\,\mu m^{-1}$) for each channel ($i$) through [1] according to Holben *et al.* (1990):

$$L_i = \alpha_i \left(DN_i - C_i \right) \qquad [1]$$

where $\alpha = 1/G_i$, G_i is the channel gain (counts/$Wm^{-2}\,sr^{-1}\,\mu m^{-1}$) and C_i is the channel offset (counts). The TOA radiance was converted to a TOA isotropic reflectance (ρ_I) by dividing by the exo-atmospheric solar irradiance ($Wm^{-2}\,\mu m^{-1}$) within each channel (E_i) normalized by the cosine of the solar zenith angle (θ_z) at time of data acquisition.

$$\rho_I = \frac{\pi L_i}{\cos\theta_z E_i} \qquad [2]$$

The filtered exo-atmospheric irradiances used were 1615 $Wm^{-2}\mu m^{-1}$ and 1032 $Wm^{-2}\mu m^{-1}$ for channels 1 and 2 respectively (Neckel and Labs, 1984; Teillet and Holben, 1992). The TOA isotropic albedos for the visible and near-infrared channel (chs. 1 and 2 respectively) are shown in Figure 2. As expected with a snow cover, reflectance was higher in the visible channel than the near-infrared (Warren, 1982). There is considerable variability between orbits that appears to be symmetrical around solar noon. Potential sources of this variability will be addressed later.

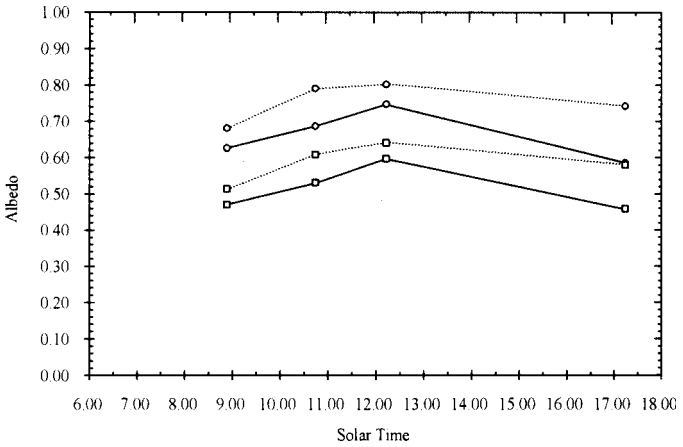

FIG. 2. Visible (o) and near-infrared (*) AVHRR albedos at the TOA under the assumption that the reflected radiance field is isotropic (—) and anisotropic (- - -).

Anisotropic Conversion: In order to relate isotropic satellite TOA reflectances to the true planetary albedo, the anisotropy of the radiation reflected by the earth-atmosphere system must be considered. Using broadband NIMBUS 7 Earth Radiation Budget (ERB) data, Taylor and Stowe (1984) determined anisotropic

correction factors (f) for TOA reflectances over various surface types, including snow and ice. Isotropic TOA reflectances can be corrected for the anisotropy of radiation reflected from the earth-atmosphere system by:

$$\rho_{TOA} = \frac{\rho_I}{f} \qquad [3]$$

where ρ_{TOA} is the anisotropically-corrected TOA reflectance. The anisotropic correction factor is dependent on the solar zenith angle, satellite zenith angle, and on the relative difference between the solar azimuth angle and the satellite azimuth angle. The conversion factors for the satellite data examined here ranged from 0.79 to 0.92 depending on the solar and viewing geometry (see Table 2). For comparison, final broadband albedos were also derived based on the assumption that the reflected radiation field is isotropic. Anisotropic TOA albedos for both channels are included in Figure 2.

TABLE 2. Koepke coefficients for AVHRR channels 1 and 2 and anisotropic conversion factor (f).

Orbit	Chn. 1 a	Chn. 1 b	Chn. 2 a	Chn. 2 b	f
5186	0.121	0.602	0.067	0.571	0.92
5187	0.107	0.628	0.058	0.590	0.87
5188	0.104	0.634	0.056	0.594	0.93
5191	0.165	0.525	0.099	0.514	0.79

Atmospheric Correction: The basis of the use of satellite measurements to determine surface albedo is the assumption that the reflected signal received at the top of the atmosphere is dominated by solar energy reflected from the earth's surface. This signal is affected, however, by atmospheric scattering and absorption processes along both the incident and reflected path length. These effects must be considered before satellite-derived TOA albedos can be converted to surface reflectance. One approach is to model the atmospheric attenuation of the satellite signal through the use of a time-consuming radiative transfer model (Tanre *et al.,* 1992). We can, however, take advantage of the following linear relationship between surface albedo (ρ_s) and TOA albedo (Chen and Ohring, 1984):

$$\rho_{TOA} = a + b\rho_s \qquad [4]$$

Using a radiative transfer model with various cloud-free model atmospheres and surface bidirectional reflectance functions, Koepke (1989) developed coefficients for a and b that are specific to AVHRR channels 1 and 2. These coefficients are functions of the solar zenith angle and atmospheric parameters specific to each channel. In channel 1, the aerosol optical depth (at 0.55 μm) is specified as either a clear (0.05) or turbid (0.4) atmosphere with total ozone thicknesses of 0.24 or 0.36 cm at normal temperature and surface pressure (NTP). In channel 2, the aforementioned optical depths can be combined with water vapour amounts of 0.5, 2 or 5 g·cm^{-2}. In order to decide on the appropriate atmospheric parameters, *in situ* observations were used when available. Values that were intermediate to the Koepke values were derived by simple linear interpolation.

Koepke's aerosol optical depths were evaluated at 0.55 μm. Therefore, total optical depth values determined through hourly sun photometer measurements collected in the field at 0.5 μm were used to choose the appropriate Koepke coefficient. Based on Leckner's (1978) approximations, aerosol optical depth was determined by subtracting the contributions of Rayleigh scattering and gaseous absorption from the total optical depth. A Rayleigh optical depth of 0.145 was calculated for dry air at sea level. In the case of gaseous absorption, ozone was the only gas considered for the 0.5 μm data. Using values based on an atmospheric ozone amount of 0.4 cm (NTP) (Rossow *et al.,* 1991), the optical depth of ozone absorption was calculated at 0.012 (Robinson, 1966; Iqbal, 1983). The resultant aerosol optical thickness for day 134 at 0.5 μm was 0.303. Although the atmosphere was cloud-free, an aerosol depth of 0.303 suggests that it was still somewhat turbid and larger than that attributed to the spring aerosol loading of the arctic atmosphere (Shaw, 1982). Airborne photometer measurements collected during the 1992 Lead Experiment (LEADEX) in the Beaufort Sea revealed stratospheric optical depths of approximately 0.1, which is a magnitude higher than normal. These larger than normal optical depths are attributed to suspended volcanic ash in the lower stratosphere originating from the 1992 eruption of Mt. Pinatubo in the Philippines (Stone *et al*., 1993).

In the case of the atmospheric ozone content, Koepke's coefficients are based on amounts of 0.24 and 0.36 cm (NTP). An ozone amount of 0.36 cm (NTP) was considered to be most appropriate for that latitude at that time of year (May, June) (Rossow *et al.,* 1991). For the atmospheric water vapour amount in a vertical column, Koepke considered three values: 0.5, 2 and 5 g·cm^{-2}. A water vapour amount of 0.5 g·cm^{-2} was chosen, consistent with the calculated water vapour amount from daily radiosonde profiles originating from the AES Resolute Bay weather station.

In Figures 3(a) and 3(b), narrowband TOA albedos and atmospherically-corrected surface albedos are shown for both the isotropic and anisotropic TOA cases respectively. Over highly reflective surfaces like ice, TOA albedo measurements are expected to underestimate surface albedo due to the forward

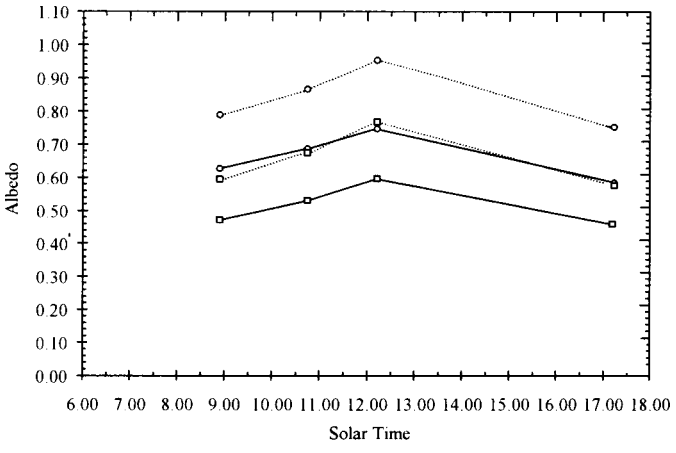

FIG. 3(a). Visible (o) and near-infrared (*) AVHRR albedos at the TOA (—) and at the surface (- - -) under the assumption that the reflected radiance field is isotropic.

scattering of aerosols. The atmospheric correction accounts for this by increasing the TOA albedo by 27 to 32% for both channels. In the anisotropic case, removing the atmospheric effects results in an albedo just over one in the visible channel for the orbit closest to solar noon. In this case, the coefficients used appear to overcorrect the TOA albedo.

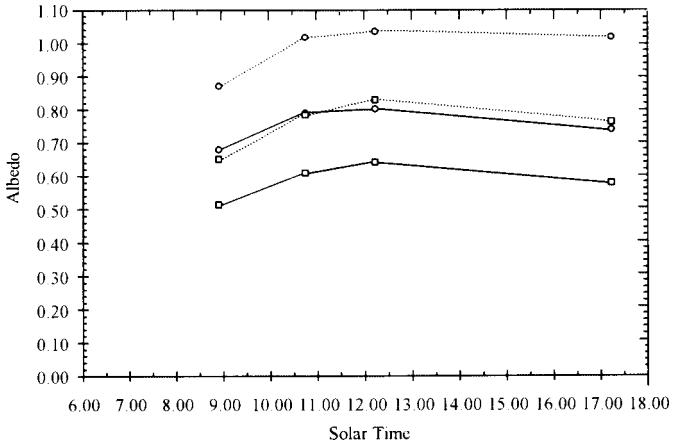

FIG. 3(b). Visible (o) and near-infrared (*) AVHRR albedos at the TOA (—) and at the surface (- - -) under the assumption that the reflected radiance field is anisotropic.

Narrow to Broadband Conversion: For climatological purposes, it is desirable to employ a surface albedo measurement that represents surface reflectance integrated over the entire solar spectrum. This is commonly referred to as a broadband or climatological albedo (α). In order to utilize surface albedos measured over narrowband channels like the AVHRR, a conversion to a broadband albedo is required. Using coincidental narrow and broadband satellite data, a linear relationship of the following form relating AVHRR channel 1 and channel 2 reflectances (ρ_1 and ρ_2 respectively) to a broadband surface albedo has been developed (Wydick *et al.,* 1987; Li and Leighton, 1992):

$$\alpha = c + d_1\rho_1 + d_2\rho_2 \qquad [5]$$

Unlike Wydick *et al.* (1987), Li and Leighton (1992) used datasets collected on the same platform, thus ensuring a higher degree of coincidence and collocation. Broadband Earth Radiation Budget Experiment (ERBE) and narrowband AVHRR data from NOAA 9 were used to determine regression coefficients for the conversion. Secondly, the authors accounted for the effect of spatial autocorrelation in the regression results. Finally, and more importantly to our investigation, the study area was located in a region north of 60°N. Thus, Li and Leighton's values for ice/snow will be used for the conversion. Equation 5 then becomes:

$$\alpha = 0.0453 + 0.389\rho_1 + 0.452\rho_2 \qquad [6]$$

Li and Leighton give a relative error (ratio of RMS error over the mean measured broadband reflectance) of 4.5% for the performance of the model over ice/snow surfaces. This was the lowest error among the various scene types investigated. For the sake of comparison, Wydick *et al.*'s conversion was applied to the narrowband data and compared to the results derived from [6]. On average, Li and Leighton's conversion produced albedos 4.6% higher than those calculated using Wydick *et al.*'s conversion.

RESULTS

Surface Albedo

The purpose of the albedo transects was to determine the magnitude and variability of surface albedo over an area typical of an AVHRR pixel. Mean surface albedo for transect observations at the 1 × 1 km site during May was 0.87, with maximum day-to-day variability of about 5% (Fig. 4). The albedo values are in general agreement with previous measurements over snow surfaces (Carrol and Fitch, 1981; Warren, 1982; Wendler and Kelly, 1988). Surface albedo increased during our initial observations from day 129–131, associated with light snowfall or ice crystal precipitation, then decreased from 0.89 to 0.85 from day 134–139 as the snowpack aged. Albedo then increased again on day 142 following new snowfall. For day 134, the mean grid albedo was 0.89 (standard deviation, SD = 0.03).

Variability within some individual transects was quite high (Fig. 4). Since the albedometer yielded stable albedo readings at individual stops, we attribute this inter-stop variability to changes in the surface condition, particularly the small linear snow drifts (e.g., sastrugi-like features) along the transects, combined with variations in cloud cover during the sampling period. While an effort was made to conduct sampling under stable irradiance conditions, conditions would change during the time required to cover the grid. Cloud cover modulates incident radiation by changing its spectral composition and incident geometry, ultimately affecting the surface albedo. However, due to the high zenith angles and dynamic cloud cover in the Arctic, it is very difficult to isolate the effect of cloud cover on surface albedo (Wiscombe and Warren, 1980; Carrol and Fitch, 1981).

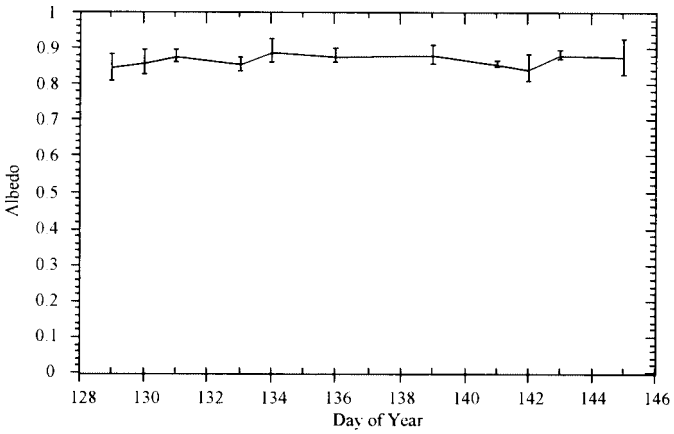

FIG. 4. Mean surface albedo of the NOAA grid. (error bars represent ±one standard deviation)

AVHRR-Derived Albedo

Mean subarea values of surface broadband albedos were determined for each pass on day 134. Figure 5 shows these average broadband albedos calculated with and without a correction for anisotropy. Beginning with the earliest pass, the resultant broadband surface albedos for data *not* corrected for anisotropy were 0.62 (SD = .006), 0.69 (SD = .003), 0.76 (SD =.003), and 0.60 (SD = .003). For data corrected for anisotropy the results were 0.68 (SD = .006), 0.80 (SD = .003), 0.82 (SD = .003), and 0.79 (SD = .004). It is obvious that the application of the anisotropic model improved the magnitude and variability of the derived surface albedo for day 134. Even after the correction for viewing geometry, there was still some residual variability between the orbits. *In situ* measured surface albedos coincidental to the satellite overpasses are superimposed on Figure 5 for comparison to the AVHRR-derived albedos. The earliest measurement of 0.89 (SD = 0.034) is the mean grid albedo for the NOAA grid. A fresh 2 cm layer of snow had fallen overnight and is likely responsible for the high surface albedos measured in the morning. Also, since snow albedo has been shown to have a slight dependence on solar zenith angle (Warren, 1982), a higher surface albedo is expected during high morning and evening zenith angles. The later measurement of 0.86 (SD = 0.022) was measured over the 500 m × 500 m SAR grid located at the FYI site. The time series measurement throughout the experiment day is from the FYI site tower (mean α = 0.81, SD = 0.008). After comparing the surface data to the satellite-derived albedo measurements, the results are positive. In all but the earliest pass, the data corrected for viewing geometry were in close agreement with the surface observations, especially those from the climate tower. The satellite albedos not corrected for anisotropy all underestimated the surface albedo.

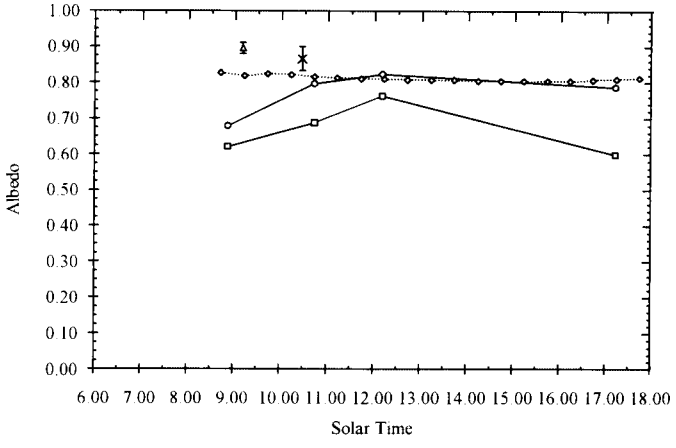

FIG. 5. AVHRR-derived surface broadband albedo for the isotropic (˚) and anisotropic case (o). Surface-based albedo measurements are superimposed: 1 km × 1km sampling grid (Δ), 500 m × 500 m grid (C) and climate tower (-◊-) (error bars represent ±one standard deviation)

DISCUSSION

This investigation has highlighted various issues relating to the retrieval of surface broadband albedo over arctic sea ice. Some of these issues are universal to the retrieval of surface fluxes regardless of geographic location; however, it is apparent that the arctic environment presents unique challenges to measuring surface broadband albedo from AVHRR narrow-band data.

Surface Validation

Surface validation is critical to the development, evaluation and evolution of retrieval methodologies for remotely sensed data. However, its value to the overall process is directly related to our ability to measure pertinent variables over appropriate spatial, temporal and spectral resolutions with a high degree of accuracy. Within this investigation, transect measurements were performed coincident with AVHRR overpasses to assess the spatial variability of surface albedo and thus allow for the later assessment of the accuracy of a satellite-retrieved albedo. The large degree of variability within sampling transects is a testament to the difficulty in measuring albedo over large spatial areas. In order to evaluate the magnitude and variability of surface albedo over the sampled grid, the contribution of the atmosphere and measurement error has to be considered. Unfortunately, this type of sampling required the radiometers to be set up several times over the transect increasing the opportunity for such error. Sources of this error are variations in instrument height, orientation to solar principal plane, shadowing and sensor leveling. More importantly, the grid transects required 1.5 – 2 hours to complete; a period over which irradiance conditions often changed. Thus, often an average albedo measurement over a sampling grid would not only represent the variability in surface conditions, but in the atmosphere as well. A more attractive option is measurement made from a height that would allow for an instantaneous measurement of a surface albedo that integrates a large surface area. Possible platforms for such measurements could be low-flying aircraft and/or balloon measurements.

Sensor Calibration

A serious problem facing the use of AVHRR data to determine shortwave radiative fluxes of the earth-atmosphere system is the absence of on-board calibration of the sensor's visible and near-infrared channels. As a result, preflight calibration coefficients, sensitive to sensor drift due to the space environment, must be relied upon (Holben *et al.,* 1990). These preflight calibrations are accurate to about 5 – 10% (Brest and Rossow, 1992). A desire for more accurate inflight calibrations has led to the development of various land and aircraft-based calibration procedures (Teillet and Holben, 1992). These investigations have shown a significant decrease in the sensitivity of the sensor's visible and near-infrared channels with time in orbit. Teillet and Holben (1992) synthesized the results of previous inflight calibration programs and developed a time-dependent correction for the pre-flight calibrations for NOAA 6 – 11. No correction is offered for NOAA 12, probably due to the fact that no inflight calibration information was yet available, for at the time of data acquisition, NOAA 12 had been in orbit for only 364 days. Since the drift in instrument calibration expected over this short time would be

small, the magnitude of error in the surface broadband calculation is considered minor.

Anisotropic Correction

While relatively isotropic over small zenith angles, the reflected radiance from snow-covered sea ice has been found to be anisotropic at polar latitudes due to consistently large zenith angles and the properties of the snow/ice surface. By showing that surface albedo is considerably underestimated when the reflected radiance field is assumed to be isotropic, this study has highlighted the importance of anisotropic correction of satellite data collected over polar surfaces. Figure 2 illustrates the effect of the anisotropic correction for both the visible and near-infrared channels. While there is considerable variability between consecutive passes for both days, anisotropic correction increased the magnitude (26–28%) and reduced the diurnal variability of the TOA albedo. The correction of the first pass (#5186) appears unable to account for the viewing geometry. The source of the residual variability between orbits is likely due to error in the anisotropic and/or atmospheric correction of the satellite data.

While it appears that they have improved the surface albedo estimates, the applicability of Taylor and Stowe's (1984) anisotropic coefficients to this investigation merits attention. Koepke and Kriebel (1987) point out that Taylor and Stowe's (1984) factors were computed using coarse resolution data (250 km^2) and suggest the use of regional anisotropic conversion factors if the area of interest deviates from the size of the study's zonal average and is heterogeneous in detail (e.g., vegetated surfaces). Given the relative homogeneity of the study site and the surrounding region during the time of data acquisition, Taylor and Stowe's (1984) conversion factors are assumed to be appropriate. However, due to the transformation of the sea ice surface during melt conditions, this assumption of homogeneity is likely invalid later in the melt season. It should also be noted that these coefficients were developed for a broadband sensor response and here they are applied to individual narrowband channels based on the assumption that the anisotropic behavior of the earth and atmosphere is the same for both channels. The validity of this assumption is difficult to determine due to the lack of information regarding the wavelength-dependence of the anisotropy in the earth-atmosphere system, although for a snow surface there is some observational evidence that the anisotropic correction is not significantly different for the two channels (K. Steffen, pers. comm. 1992). Compared to other land types examined by Taylor and Stowe (1984), the variability within the angular bins used to calculate the snow and ice coefficients was relatively low, thus reducing the magnitude of error in f.

While it is difficult to assess the accuracy of Taylor and Stowe's (1984) anisotropic coefficients, we can borrow from the investigation of Koepke and Kriebel (1987) and comment on the error in deriving surface albedo using a model in the form of [4] given a certain level of uncertainty in the anisotropic conversion coefficient. Given an approximate difference of -0.075 between the true and assumed values of f and a surface reflectance of 0.88, the derived surface albedo would have an error of 0.09 and 0.11 based on applying the f coefficients of 0.83 and 1.0 respectively (based on solar zenith angle of 57.5°, water vapour amount of 2 $g \cdot cm^{-2}$ and an aerosol optical depth (0.55 μm) of 0.4). In other words, the estimated albedo would be too low. If calculated under a clear atmosphere (aerosol optical depth 0.05), the surface albedo would be in error by 0.08 and 0.095 based on the same two f coefficients mentioned above. The error in surface albedo due to uncertainty in f appears to increase with surface reflectance and decrease with atmospheric turbidity. It is apparent that the accuracy of a surface albedo derived from an inversion model such as [4] is very sensitive to the accuracy of the anisotropic coefficient employed.

Given its demonstrated importance, the magnitude and wavelength dependence of anisotropy needs to be investigated over various polar surfaces and incorporated into future inversion efforts. The Taylor and Stowe (1984) model was derived under very general conditions over coarse resolutions and offers correction factors that represent large ranges of angles. This could be the major source of the residual variability within the daily cycle after the application of the model. Also, the extension of the model to both the narrowband visible and near-infrared band needs to be examined fully. Of further concern is the sensitivity of this model to the seasonal evolution of the ice surface. Although homogeneous for much of the spring, surface melt transforms the sea ice surface into a heterogeneous mix of melt ponds, bare ice and open water, thus likely invalidating the use of Taylor and Stowe's model during this part of the season. This highlights the need for bidirectional reflectance surface and atmospheric models that are sensitive to the seasonal and spatial variations of the reflectance of sea ice surfaces.

Atmospheric Correction

Due to large solar zenith angles, air masses characteristic of polar atmospheres increase the attenuation of both incident and reflected radiation. Over long path lengths, aerosol scattering and water vapour absorption take on increased significance by modulating the incident and reflected radiation signal. This is evident when comparing TOA albedos to surface albedos after atmospheric correction. While the results of the investigation seem to generally validate the use of Koepke's (1989) coefficients for the atmospheric correction of this dataset, the following should be noted before extending the model to other high-latitude AVHRR data. After considering the atmospheric conditions during data collection, the validity of the aerosol behavior in the model is uncertain given the presence of clear sky phenomena such as suspended ice crystal ("diamond dust") events and aged volcanic ash. The continental aerosol model used in Koepke's (1989) model has an absorption fraction of 0.11. Typical arctic aerosols have absorption fractions of 0.08 (relative humidity of 70%), thus absorbing less and scattering more (Blanchet and List, 1983). The sensitivity of our estimated surface albedo to errors in the prescribed absorption of aerosols can be determined by examining the results of Koepke and Kriebel (1987). An error of 0.05 in the aerosol absorption fraction (i.e., the presumed value is too low) will result in the surface albedo being underestimated by 0.09 under turbid conditions and 0.01 under clear conditions. The authors show

that the error in the fractional amount of aerosol absorption is the largest contributor to the overall error in surface albedo caused by the atmospheric correction of the satellite data. Uncertainty in the prescription of optical depth and water vapour only moderately contribute to the overall error. Future work will focus on isolating these individual effects through a combination of field observations and modeling.

Spectral Response

In order to derive broadband albedo from narrowband AVHRR data, a conversion that takes into account the relative response in both channels is necessary. In this investigation, a linear model based on the relationship between TOA broadband and TOA narrowband albedos was used (Li and Leighton, 1992) to derive surface broadband albedos. The appropriateness of extending the TOA conversion to surface estimates of albedo, as done in this study, is unknown. Using the 5S radiative transfer model (Tanre *et al.*, 1990), the magnitude of error involved with such an extension was assessed. Two standard atmospheric profiles, subarctic summer and mid-latitude summer, were used to examine the change in relationship between channel 1 and channel 2 as one moves from the surface to the TOA. The surface albedo was taken from Warren and Wiscombe's (1980) calculations and the broadband conversion was based on Li and Leighton's (1992) formulation. Table 3 shows the difference between the channel 2/channel 1 ratio at the TOA and surface. As expected, the ratios differ due to scattering and absorption processes in the atmosphere. Increasing the water vapour amount (illustrated here by using the mid-latitude rather than the subarctic standard profile) decreases the TOA channel 2 albedo, while changing aerosol or ozone amounts does not make a large difference in the TOA ratios. Assuming that the atmospheric correction was correct, the broadband error cited in Table 3 (approx. 2–3%) refers to the magnitude of error expected in surface broadband albedos derived with Li and Leighton's TOA conversion coefficients. Since the reflectance of a sea ice cover is seasonally dependent, the relationship between channel 1 and channel 2 will change with the appearance of melt ponds and open leads. Also, seasonal changes in relative humidity will result in differing atmospheric water vapour amounts. Consequently, any broadband conversion scheme will have to be sensitive to the seasonal changes at the surface, as well as in the atmosphere.

SUMMARY AND CONCLUSIONS

The results of this investigation are considered an evolutionary step towards understanding the issues involved in the utilization of AVHRR data to derive surface albedo over sea ice. This examination has shown the importance of atmospheric and anisotropic correction when deriving surface albedos from high-latitude AVHRR satellite data. While the results appear to validate the general methodology given this particular dataset, questions remain regarding the magnitude and variability of the derived albedos over the experiment day. Given the generalities of the anisotropic ice model and the assumptions involved with the atmospheric correction, the magnitudes of the difference between the surface observations and the AVHRR-derived products between consecutive orbits is not surprising. Uncertainty due to the anisotropy of the radiance field and the masking effect of the overlying atmosphere is significant and at its highest over polar surfaces. It is evident that most of the uncertainty in this approach lies in accounting for the effects of the atmosphere and the anisotropy of the snow/ice surface. Under typical cloud-free conditions (i.e., small atmospheric optical depth), we would expect the derived surface albedo to be most sensitive to the anisotropic correction of the satellite data. Taylor and Stowe's (1984) anisotropic model improved our surface albedo estimates, but it is evident that more work is needed in order to account for the anisotropy of the reflected radiance field due to variations in the sun-target-sensor geometry between satellite orbits.

Although the experiment day was relatively cloud-free, the presence of atmospheric aerosols was considerable.

TABLE 3. Modelling of broadband albedo at the TOA and surface.

Profile	Aerosol[3]	Surface Albedo Ch. 1	Surface Albedo Ch. 2	Surface Ratio Ch.2/Ch.1	TOA Albedo Ch. 1	TOA Albedo Ch. 2	TOA Ratio Ch.2/Ch.1	Error
SS	0.3	0.85	0.62	0.729	0.68	0.45	0.664	0.025
SS	0.1	0.85	0.62	0.729	0.73	0.48	0.662	0.026
MS	0.3	0.85	0.62	0.729	0.68	0.44	0.644	0.033
MS	0.1	0.85	0.62	0.729	0.73	0.47	0.642	0.034

[1] SS = subarctic summer (water vapour = 2.1 g·cm^2; O_3 = 0.346 cm-atm).

[2] MS = mid-latitude summer (water vapour = 2.93 g·cm^2; O_3 = 0.319 cm-atm).

[3] Aerosol refers to aerosol optical depth.

Notes:

- Viewing geometry: solar zenith, satellite zenith and relative azimuth angle are 60°, 20° and 65° respectively.
- Surface albedo from Warren and Wiscombe (1980) for diffuse and direct beam with ice-crystal radius = 1000 μm, soot concentration =1 ppmw and a 1 μm particle radius for the direct beam case (at 0.6 and 0.9 μm for ch. 1 and ch. 2).
- Broadband calculation based on Li and Leighton (1992). The error is the difference between the broadband albedo calculated using the surface albedo (no atmosphere), and that computed using a hypothetical TOA albedo in ch. 1 equal to the surface albedo and with ch. 2 equal to ch.1 scaled by the TOA ratio.

Stratospheric aerosols and boundary layer ice crystals increase the sensitivity of the estimated surface albedo to errors in the atmospheric correction of the data. This is more true over the long atmospheric path lengths of the morning and evening hours. In light of the scarcity of cloud-free data in the Arctic, the ability to utilize a clear-sky pass regardless of overpass time is attractive. This requirement will demand a more complete understanding of the role of the atmosphere in the modulation of the incident and reflected signal, along with an improved comprehension of the effects of viewing geometry on the reflected signal. This investigation has also highlighted the difficulty in measuring spatially-representative *in situ* surface albedos for comparison to satellite imagery.

Future investigations will be characterized by a strong field and modeling component. Field sampling will focus on both the surface and atmosphere. More specifically, a concerted effort will be made to characterize the spatial and temporal (diurnal and seasonal) variability of both spectral and integrated albedo over first and multi-year ice surfaces. Also, the effects of high cirrus clouds and diamond dust events on the extinction of irradiance will be examined. The results of this investigation will be further examined through the incorporation of coincidental spectral reflectance and irradiance measurements, along with a more explicit treatment of the atmosphere through a radiative transfer approach.

ACKNOWLEDGEMENTS

This work was supported by funding through the following agencies: the National Science and Engineering Research Council (Postgraduate scholarship - R. De Abreu, Operating Grant - E. Le Drew), the U.S. National Science Foundation (Grants NSF/DPP 9113958 - M. Serreze and 9024114 - J. Maslanik), NASA (Grant NAGW-2407 - J. Key and NAGW-2158 - K. Steffen), the Institute for Space and Terrestrial Science, Center of Excellence (Contract - E. LeDrew) and the Northern Studies Scientific Training Program (Grant - R. De Abreu). The authors wish to extend their appreciation to the Atmospheric Environment Service for providing the AVHRR data, the SIMMS experiment team and finally to the reviewers for their helpful comments.

REFERENCES

BLANCHET, J-P., and LIST, R. 1983. Estimation of optical properties of Arctic haze using a numerical model. Atmosphere-Ocean 21(4):444–465.

BREST, C.L., and Rossow, W.B. 1992. Radiometric calibration and monitoring of NOAA AVHRR data for ISCCP. International Journal of Remote Sensing 13(2):235–273.

BUDYKO, M.I. 1969. The effect of solar radiation variations on the climate of the Earth. Tellus 21:611–619.

CARLETON, A.M. 1991. Satellite remote sensing in climatology. Boston: Bellhaven Press. 291 p.

CARROL, J.J., and FITCH, B.W. 1981. Effects of solar elevation and cloudiness on snow albedo at the South Pole. Journal of Geophysical Research 86(C6):5271–5276.

CHEN, T.S., and OHRING, G. 1984. On the relationship between clear-sky planetary and surface albedos. Journal of Atmospheric Science 41:156–158.

CUBASCH, V., and CESS, R.D. 1990. Processes and modeling. In: Houghton, J.T., Jenkins, G.J., Ephraumus, J.J., eds. Climate change, the IPCC scientific assessment. Cambridge: Cambridge University Press. 364 p.

GUTMAN, G. 1988. A simple method for estimating monthly mean albedo of land surfaces from AVHRR data. Journal of Applied Meteorology 27:973–988.

HOLBEN, B.N., KAUFMAN, Y.J., and KENDALL, J.D. 1990. NOAA-11 AVHRR visible and near-IR inflight calibration. International Journal of Remote Sensing 11(8):1511–1519.

IQBAL, M. 1983. An introduction to solar radiation. Toronto: Academic Press. 390 p.

KIDWELL, K.B. 1991. NOAA polar orbiter data users guide. Washington, D.C.: U.S. Department of Commerce, NOAA NESDIS. 250 p.

KOEPKE, P. 1989. Removal of atmospheric effects from AVHRR albedos. Journal of Applied Meteorology 28(12):1341–1348.

KOEPKE, P., and KRIEBEL, T. 1987. Improvements in the shortwave cloud-free radiation budget accuracy. Part I: Numerical Study Including Surface Anisotropy. Journal of Climate and Applied Meteorology 26:374–395.

LATIMER, J.R. 1972. Radiation Measurement. International Field Year for the Great Lakes Technical Manual Series No. 2. Ottawa: National Research Council of Canada. 53 p.

LECKNER, B. 1978. The spectral distribution of solar radiation at the earth's surface–elements of a model. Solar Energy 20(2): 143–150.

LeDREW, E.F., and BARBER, D.G. 1994. The SIMMS program: A study of change and variability within the marine cryosphere. Arctic 47(3): 256–264.

LI, Z., and LEIGHTON, H.G. 1992. Narrowband to broadband conversion with spatially autocorrelated reflectance measurements. Journal of Applied Meteorology 31:421–432.

NECKEL, H., and LABS, D. 1984. The solar radiation between 3300 and 12500 Å. Solar Physics 90:205–258.

REDDAN, S., BARBER, D.G., and LeDREW, E. F. 1992. SIMMS'92 Data report ISTS-EOL-SIMMS-TR92-003. Waterloo: Earth Observations Laboratory, ISTS and the Department of Geography, University of Waterloo, Waterloo.

ROBINSON, N. 1966. Solar Radiation. New York: American Elsevier.

ROSSOW, W.B., GARDER, L.C., LU, P-J., and WALKER, A. 1991. International Satellite Cloud Climatology Project Documentation of Cloud Data. WMO/TD-No. 266. Geneva: World Meteorological Organization. 78 p. + appendices.

SAUNDERS, R.W. 1990. The determination of broad band surface albedo from AVHRR visible and near-infrared radiances. International Journal of Remote Sensing 11(1):49–67.

SELLERS, W.D. 1969. A global climatic model based on the energy balance of the Earth-Atmosphere system. Journal of Applied Meteorology 8:392–400.

SHAW, G. E. 1982. Atmospheric turbidity in the polar regions. Journal of Applied Meteorology 21:1080–1088.

STEPHENS, G.L., CAMPBELL, G.G., and VONDER HAAR, T.H. 1981. Earth radiation budgets. Journal of Geophysical Research 86:9739–60.

STONE, R.S., KEY, J.R.,and DUTTON, E.G. 1993. Properties and decay of stratospheric aerosols in the Arctic following the 1991 eruptions of Mount Pinatubo. Geophysical Research Letters 20 (21):2359–2362.

TANRE, D., DEROO, C., DUHAUT, P., HERMAN, M., and MORCRETTE, J.J. 1990. Description of a computer code to simulate the satellite signal in the solar spectrum: the 5S code. International Journal of Remote Sensing 11(4):659–668.

TANRE, D., HOLBEN, B.N., and KAUFMANN, Y.J. 1992. Atmospheric correction algorithm for NOAA-AVHRR products: Theory and application. IEEE Transactions on Geoscience and Remote Sensing 30 (2): 231–248.

TAYLOR, V.R., and STOWE, L.L. 1984. Atlas of reflectance patterns for uniform earth and cloud surfaces (NIMBUS-7 ERB – 61 days). NOAA Technical Report NESDIS 10. 66 p.

TEILLET, P.M., and HOLBEN, B.N. 1992. A multi-level electronic database for documentation and dissemination of time-dependent NOAA-AVHRR calibration coefficients for the solar reflective channels. 6th Australasian Remote Sensing Conference, Wellington, New Zealand. November.

WARREN, S.G. 1982. Optical properties of snow. Reviews of Geophysics and Space Physics 20(1):67–89.

WARREN, S.G., and WISCOMBE, W.J. 1980. A model for the spectral albedo of snow. II: Snow containing atmospheric aerosols. Journal of Atmospheric Sciences 37:2734–2745.

WENDLER, G., and KELLEY, J. 1988. On the albedo of snow in Antarctica: A contribution to I.A.G.O. Journal of Glaciology 34(116):19–25.

WISCOMBE, W.J., and WARREN, S.G. 1980. A model for the spectral albedo of snow. I: Pure snow. Journal of Atmospheric Sciences 37:2712–2733.

WYDICK, J.E., DAVIS P.A., and GRUBER, A. 1987. Estimation of broadband planetary albedo from operational narrowband satellite measurements. NOAA Technical Report NESDIS 27. 32 p.